Stem Cell Research & Therapy

RESEARCH

Open Access

Extracellular vesicles derived from mesenchymal stem cells alleviate renal fibrosis via the miR-99b-5p/mTOR/autophagy axis in diabetic kidney disease

Rongrong Li[1,2,3†], Hongyan Tao[2†], Kai Pan[2,3], Rui Li[2], Zhikun Guo[1,3], Xiaoniao Chen[4,5*] and Zongjin Li[1,2,3,5*]

Abstract

Background Diabetic kidney disease (DKD) is the leading cause of end-stage renal disease (ESRD) globally, presenting a significant therapeutic challenge. Extracellular vesicles (EVs) from mesenchymal stem cells (MSCs) have emerged as promising therapeutic agents. This study explored the therapeutic effects and mechanisms of EVs derived from human placental mesenchymal stem cells (hP-MSCs) on DKD.

Methods EVs were isolated from cultured hP-MSCs and administered to streptozotocin (STZ)-induced diabetic mice and high glucose–treated glomerular mesangial cells. The therapeutic impact of EVs was assessed through histological analysis and biochemical assays. miR-99b-5p expression in EVs and its role in modulating the mechanistic target of rapamycin (mTOR)/autophagy pathway were examined via western blotting and RT–qPCR.

Results Treatment with hP-MSC-derived EVs significantly alleviated renal fibrosis and improved renal function in DKD models. These EVs were enriched with miR-99b-5p, which targeted and inhibited mTOR signaling, thereby increasing autophagic activity and reducing cellular proliferation and extracellular matrix accumulation in renal tissues.

Conclusions hP-MSC-derived EVs can mitigate renal injury in DKD by modulating the miR-99b-5p/mTOR/autophagy pathway. These findings suggest a potential cell-free therapeutic strategy for managing DKD.

Keywords Diabetic kidney disease (DKD), Glomerular mesangial cells, Extracellular vesicles, Mesenchymal stem cells, miR-99b-5p, mTOR

†Rongrong Li and Hongyan Tao contributed equally to this work.

*Correspondence:
Xiaoniao Chen
birdchen512@qq.com
Zongjin Li
zongjinli@nankai.edu.cn
[1]Henan Key Laboratory of Cardiac Remodeling and Transplantation, Zhengzhou Seventh People's Hospital, No. 17 Jingnan 5th Road, 450016 Zhengzhou, China
[2]School of Medicine, Nankai University, 94 Weijin Road, 300071 Tianjin, China
[3]Henan Key Laboratory of Medical Tissue Regeneration, Xinxiang Medical University, Xinxiang, China601 Jinsui Road, 453003
[4]Department of Ophthalmology, The Third Medical Center of Chinese PLA General Hospital, 69 Yongding Road, Beijing 100039, China
[5]National Key Laboratory of Kidney Diseases, Chinese PLA General Hospital, 28 Fuxing Road, 100853 Beijing, China

Introduction

Diabetic kidney disease (DKD), the most severe microvascular complication of diabetes, is the leading cause of end-stage renal disease (ESRD) and is related to markedly increased morbidity and mortality of cardiovascular disease worldwide [1–3]. The prominent pathological manifestations of DKD are glomerular hypertrophy, thickening of the basement membrane and mesangial expansion, which are caused by mesangial cell remolding, eventually leading to glomerulosclerosis [4]. Glomerular mesangial cells, which maintain extracellular matrix (ECM) homeostasis, regulate the glomerular filtration rate, clear debris, and play pivotal roles in preserving glomerulus structure and renal function [5, 6]. Under diabetic conditions, glomerular mesangial cells undergo cell remodeling, resulting in abnormal cell proliferation, excessive synthesis of ECM, and impaired contractile function, all of which contribute to the onset and progression of DKD [6, 7]. Therefore, exploration of the underlying mechanisms leading to mesangial dysfunction and the development of effective therapeutic strategies for preventing glomerular mesangial cell remolding to improve DKD are urgently needed.

Autophagy is an evolutionarily conserved catabolic process in which damaged organelles and protein aggregates are degraded in lysosomes to maintain cellular homeostasis or adapt to cellular stress [8, 9]. Emerging evidence suggests that dysregulation of autophagy is involved in the pathogenesis of DKD [9–12]. Owing to diabetes-related metabolic disorders, impaired autophagy contributes to the accumulation of damaged organelles and proteins in diabetic kidney cells, resulting in the development of DKD, whereas increased autophagy alleviates DKD [12–14]. The mechanistic target of rapamycin (mTOR) is considered a critical regulator of autophagy. The nutrient-sensing pathway, the mTOR signaling pathway, is hyperactivated and participates in the pathogenesis of DKD via negatively regulating autophagy [15–18]. Promoting autophagy via the suppression of mTOR markedly decreases hypertrophy, inflammation, and fibrosis and ameliorates DKD [12, 19, 20], suggesting that blocking the mTOR-mediated suppression of autophagy may be a promising therapeutic strategy to prevent DKD.

MSCs, a promising cell therapy strategy in tissue repair and regenerative medicine, exert their therapeutic effects, including immune regulation, antifibrosis effects and the promotion of tissue regeneration via direct differentiation and paracrine functions [21–23]. Recent studies have indicated that the therapeutic potential of MSCs relies mainly on EVs secreted by MSCs [24, 25]. Extracellular vesicles (EVs), which are membrane-packed nanovesicles, mediate intercellular communication by transferring cargos (miRNAs, circular RNAs, proteins and lipids) to target cells and are a cell-free therapy alternative, with the advantages of preventing immunogenicity, tumorigenicity, easy storage and production, and passing through biological barriers [3, 26, 27]. Studies have shown that MSC-EVs can yield beneficial therapeutic effects on DKD [28, 29]. However, the underlying mechanisms by which MSC-EVs alleviate DKD remain to be fully elucidated.

In this study, we investigated the therapeutic effect of hP-MSCs on DKD, as well as the underlying mechanisms by which hP-MSC-derived EVs alleviate DKD. First, we evaluated the renoprotective and antifibrotic functions of MSC-EVs after multiple infusions of MSC-EVs into DKD model mice. Furthermore, we explored the mechanisms by which MSC-EVs inhibited glomerular mesangial cell proliferation and ECM accumulation. Finally, we revealed the bioactive molecules in MSC-EVs that could regulate mTOR-mediated autophagy in vivo and in vitro. Our study provides a theoretical basis and preclinical evidence for the application of MSC-derived EV-based cell-free therapy in DKD.

Materials and methods

Cell culture

Human placenta-derived mesenchymal stem cells (hP-MSCs), purchased from AmCellGene Co. Ltd. (Tianjin, China), were cultured in line with previous reports [30–32]. Briefly, hP-MSCs were maintained in Dulbecco's modified Eagle medium/nutrient mixture F-12 (DMEM/F-12; Gibco, Grand Island, NY) supplemented with 10% fetal bovine serum (FBS; Gibco), 100 U/mL penicillin and 100 μg/mL streptomycin (Gibco) at 37 °C in 5% CO_2. In this study, hP-MSCs at passages 4 to 10 were used. Mouse glomerular mesangial cells (mMCs; the murine SV40-transfected mouse mesangial cell line SV40 MES13), purchased from the Cell Bank Type Culture Collection of the Chinese Academy of Sciences (Shanghai, China), were cultured in DMEM/F-12 supplemented with 5% FBS, 100 U/mL penicillin and 100 μg/mL streptomycin at 37 °C in 5% CO_2. To mimic hyperglycemia in diabetes mellitus, mMCs were treated with D-glucose (Sangon Biotech, China) at normal (5.5 mmol/L) or high (30 mmol/L) concentrations for the indicated times. Stimulation with 5.5 mmol/L D-glucose plus 24.5 mmol/L D-mannitol (Solarbio, China) was used as a control for osmolality.

Isolation and characterization of MSC-EVs

EVs were harvested from the supernatant of hP-MSCs as previously described [3, 27]. Briefly, EV-free FBS was obtained by centrifugation of FBS at 100,000 × g for 2 h. When the cell confluence reached 60-70%, hP-MSCs were cultured in DMEM/F-12 supplemented with 10% EV-free FBS, 100 U/mL penicillin and 100 μg/mL streptomycin at 37 °C in 5% CO_2 for another 2 days. Then,

the cell supernatant was collected and centrifuged at 500 × g for 10 min, 2 000 × g for 20 min and 10,000 × g for 60 min at 4 °C to remove cellular debris and apoptotic bodies. Subsequently, ultracentrifugation at 100,000 × g for 2 h was performed to pellet the EVs. To remove contaminants, EVs were resuspended in PBS and ultracentrifuged at 100,000 × g for 2 h. Finally, the precipitated EVs were dissolved in PBS and stored at -80 °C. A bicinchoninic acid (BCA) protein assay kit (Beyotime, China) was used to quantify the total protein content of the obtained EVs. The morphologies of the EVs were imaged via transmission electron microscopy (TEM, Talos L120C G2, FEI). The size distribution of the EVs was measured via the dynamic light scattering technique (ZETAPALS/BI-200SM, BROOKHAVEN). The protein expression of EV markers was determined via Western blotting.

Generation of miR-99b-5p-knockdown MSC-EVs

To identify the function of miR-99b-5p in protection against DKD-induced renal injury, miR-99b-5p was knocked down in MSC-EVs. Briefly, hP-MSCs were cultured in 6-well plates and transfected with either the inhibitor negative control or the miR-99b-5p inhibitor (100 nM, Sangon Biotech, China) via Lipofectamine 2000 Transfection Reagent (Invitrogen, USA) according to the manufacturer's instructions. After 72 h, MSC-EVs modified with either the inhibitor-negative control (EV-NC) or the miR-99b-5p inhibitor (EV-KD) were obtained from the conditioned medium.

Uptake of MSC-EVs

MSC-EVs labeled with the fluorescent lipophilic tracer Dil were obtained as previously described [33]. In brief, pelleted MSC-EVs were incubated with Dil (5 μM; Solarbio/Beyotime, China) for 15 min in the dark at 37 °C. Then, Dil-labeled EVs (Dil-EVs) were harvested via ultracentrifugation as described above. To detect the internalization of MSC-EVs, mMCs seeded on cell slides overnight were incubated with Dil-EVs (100 μg/mL) for 6 h. The DiI signals of MSC-EVs in mMCs were observed under a laser scanning confocal microscope.

Mice and animal models

In this study, C57BL/6 (male, 6-week-old) mice were purchased from Beijing Vital River Laboratory Animal Technology Co., Ltd. (Beijing, China). All the mice were housed under SPF conditions with controlled temperature (22–23 °C) and light (12 h:12 h light/dark cycle) and were given free access to food/water. All the experimental procedures for the animal studies were approved by the Institutional Animal Care and Use Committee of Nankai University and conducted in accordance with the National Institute of Health Guide for Care and Use of Laboratory Animals, 8th edition (Approval no. 20210051). The mice were grouped randomly into normal control (NC), DKD, DKD + EVs/EVs-NC and DKD + EVs-KD groups, and the number of mice in each group was determined via the Resource Equation Method. Briefly, a streptozotocin (STZ)-dependent model of DKD was established as previously described [34, 35]. To induce persistent hyperglycemia, the experimental mice were intraperitoneally administered STZ (55 mg/kg body weight; Solarbio, S8085) dissolved in 0.1 mol/L sterile sodium citrate buffer (pH = 4.5; Solarbio, C1013) following 12 h of food deprivation daily for 5 consecutive days, and the normal control mice were injected with 0.1 mol/L sterile sodium citrate buffer. Mice with fasting blood glucose (FBG) levels ≥ 300 mg/dL were considered diabetic 3 weeks after STZ administration, and FBG levels in mouse tail vein blood were monitored every 2 weeks via glucose testing strips (Sinocare, China). Then, PBS, MSC-EVs/EVs-NC or EVs-KD (100 μg/200 μL) were injected intravenously into diabetic mice weekly for 12 consecutive weeks, eight weeks after the last STZ injection. Mice that did not survive were excluded from the study. At 20 weeks after the last STZ injection, blood and 24 h urine samples were collected for biochemical analysis. The mice were subsequently euthanized by cervical dislocation under anesthesia (avertin, 2.5%, 240 mg/kg; Sigma–Aldrich, Oakville, ON, Canada), and kidney samples were obtained for further analysis. Thirty-eight mice were included in the study, with 4, 5 or 6 mice per group across 3 or 4 groups. The work has been reported in line with the ARRIVE guidelines 2.0.

Renal function analysis

The concentration of urine albumin was determined via an enzyme-linked immunosorbent assay (ELISA) for mouse albumin according to the manufacturer's instructions (Cloud-Clone Corp, China). The creatinine (Cr) levels in the urine and serum were assayed via a Cr assay kit (Nanjing Jiancheng Bioengineering Institute, China), and the blood urea nitrogen (BUN) level was measured via a BUN assay kit (Nanjing Jiancheng Bioengineering Institute, China) according to the manufacturer's instructions.

Renal histology and immunohistochemical staining

Renal samples were fixed in 4% paraformaldehyde, dehydrated with gradient ethanol, hyalinized with xylene, embedded in paraffin, and cut into 5 μm paraffin sections. After the renal paraffin sections were dewaxed and rehydrated, periodic acid Schiff (PAS) staining (Beyotime, China) and Masson's trichrome staining (Solarbio, China) were conducted for histological analysis via routine procedures. For immunohistochemical staining, renal paraffin sections were hyalinized with xylene, rehydrated with gradient ethanol and subjected to antigen retrieval with citrate buffer (pH 6.0). After endogenous

peroxidase activity was blocked, the renal sections were incubated with primary antibody against proliferating cell nuclear antigen (PCNA; 1:100; WL02208, Wanleibio, China) overnight at 4 °C and then analyzed via a universal two-step detection kit (mouse/rabbit enhanced polymer detection system) (PV-9000, ZSGB-BIO, Beijing, China) according to the manufacturer's protocol. Following counterstaining with hematoxylin, the PCNA-positive cells (brown) were observed under a light microscope.

Immunofluorescence staining

Renal samples were fixed with 4% paraformaldehyde, dehydrated with gradient sucrose solution, embedded in optimal cutting temperature (OCT) compound, and cut into 5 μm renal cryosections. Renal cryosections were permeabilized with PBS containing 0.5% Triton X-100, sealed with PBS containing 10% goat serum, and incubated with primary antibodies against α-SMA (1:200; sc-53142, Santa Cruz), fibronectin (1:200; sc-8422, Santa Cruz), and Col 4a1 (1:200; sc-517572, Santa Cruz) overnight at 4 °C. The cryosections were subsequently incubated with secondary antibodies labeled with Alexa Fluor 488 or Alexa Fluor 594 for 2 h and then counterstained with DAPI for 20 min at room temperature in the dark.

The mMCs were seeded on glass slides overnight and treated with normal glucose (NG, 5.5 mmol/L D-glucose), mannitol (MA, 5.5 mmol/L D-glucose plus 24.5 mmol/L D-mannitol), high glucose (HG, 30 mmol/L D-glucose), high glucose plus MSC-EVs (HG + EVs/EVs-NC) or high glucose plus EVs-KD (HG + EVs-KD) for 72 h. mMCs were fixed with 4% paraformaldehyde for 20 min, permeabilized with PBS containing 0.5% Triton X-100, sealed with PBS containing 10% goat serum, and incubated with primary antibodies against α-SMA (1:200; sc-53142, Santa Cruz), fibronectin (1:200; sc-8422, Santa Cruz), and Col 4a1 (1:200; sc-517572, Santa Cruz) overnight at 4 °C. Next, the mMCs were incubated with secondary antibodies labeled with Alexa Fluor 488 or Alexa Fluor 594 for 2 h and then counterstained with DAPI for 20 min at room temperature in the dark. The fluorescence of α-SMA, fibronectin and Col 4a1 in renal sections and mMCs was observed via a laser scanning confocal microscope (FV1000, Olympus, Lake Success, NY), and the fluorescence intensity of the regions of interest was measured.

Western blot analysis

The homogenized renal cortex or mMCs were lysed in radioimmunoprecipitation (RIPA) buffer (R0010, Solarbio) supplemented with protease and phosphatase inhibitors (A32961, Thermo Fisher). The concentration of total protein was quantified with a bicinchoninic acid (BCA) protein assay kit (Beyotime, China). Protein samples were separated via SDS–PAGE and transferred to polyvinylidene fluoride membranes (Millipore). After blocking with 5% fat-free milk for 2 h, the membrane strips were incubated with primary antibodies against PCNA (1:1000; WL02208, Wanleibio, China), p-mTOR (1:2000; ab109268, Abcam), mTOR (1:2000; #2972 CST), p62 (1:2000; ab109012, Abcam), LC3B (1:1000; et-1701-65, HUABIO) and β-actin (1:2000; 60008-1-lg, Proteintech) at 4 °C overnight, followed by incubation with an HRP-labeled secondary antibody at 25 °C for 1 h. The immunoreactivity of each protein band was detected via an enhanced chemiluminescence kit (ECL) (MA0186, Meilunbio, Dalian8-1-lg) under an automatic chemiluminescence image analysis system (Tanon, Shanghai, China).

Cell counting Kit-8 (CCK-8) array

A CCK-8 assay was conducted to detect cell viability according to the manufacturer's instructions (C0038, Beyotime). In brief, mMCs were seeded into 96-well plates at a density of 5×10^3/well overnight and were treated with NG, MA, HG, HG + EVs/EVs-NC or HG + EVs-KD for the indicated durations. Then, CCK-8 solution was added to each well for 2 h at 37 °C. The optical density (OD) value was measured at 450 nm via a microplate reader (Thermo Fisher Scientific).

5-Ethynyl-2′-deoxyuridine (EdU) assay

An EdU assay was performed to assess cell proliferation according to the manufacturer's instructions (C0071S, Beyotime). In brief, mMCs were seeded on glass slides in 24-well plates at a density of 1×10^4/well overnight. mMCs were treated with NG, MA, HG, HG + EVs/EV-NC or HG + EV-KD for 72 h, followed by treatment with 10 μM EdU for 2 h. Then, the cells were fixed, permeabilized, subjected to nuclear staining and photographed via a fluorescence microscope (Leica, Germany).

Total RNA extraction and quantitative real-time PCR

Total RNA was extracted from mMCs or renal cortical tissue via TRIzol reagent (Solarbio, China). cDNA was synthesized from template RNA via TransScript One-Step gDNA Removal and cDNA Synthesis SuperMix (Trans, China). Quantitative real-time PCR (RT–qPCR) was performed via Hieff qPCR SYBR Green Master Mix (No Rox) (YEASEN, China). The expression level of genes was normalized to that of β-actin. The expression level of microRNA (miRNA) was normalized to that of U6 (RiboBio, Guangzhou, China). The primers used are listed in Supplementary Table 1.

Statistical analysis

All data in this study are presented as the means ± standard errors of the means (SEMs). Statistical analyses were performed via GraphPad Prism 8.3.0 (GraphPad

Software, San Diego, CA). One-way analysis of variance (ANOVA) with post hoc Tukey's test was employed for multiple-group comparisons, and an unpaired two-tailed Student's t test was used for two-group comparisons. $P < 0.05$ was considered statistically significant.

Results

Characteristics of MSC-EVs

EVs isolated from the culture supernatant of hP-MSCs were characterized via transmission electron microscopy (TEM), dynamic light scattering (DLS), and Western blot analysis (WB). TEM revealed that the morphology of the MSC-EVs was a canonical round cup-shaped membrane structure (Fig. 1A). DLS analysis revealed that the average diameter of the MSC-EVs was 114.41 nm (Fig. 1B). Western blot analysis confirmed the expression of the EV-associated markers CD9, TSG101 and Alix, while the MSC marker calnexin was absent in EVs (Fig. 1C). The above results indicated that the EVs derived from hP-MSCs were successfully isolated.

MSC-EVs improved renal injury and fibrosis and promoted the activation of autophagy in the kidneys of STZ-induced diabetic mice

To investigate the protective role of MSC-EVs in DKD, a STZ-induced DKD mouse model was established, and 100 μg/200 μL MSC-EVs were injected into the mice via the tail vein (Fig. 2A). We first detected FBG, relative kidney weight, proteinuria, serum creatinine and blood urea nitrogen. The results revealed that the level of FBG did not obviously change in DKD mice treated with MSC-EVs, indicating that MSC-EVs had no effect on blood glucose levels (Figure S1A). The relative kidney weight, proteinuria and serum creatinine level were greater in DKD mice than in normal controls. However, with MSC-EV treatment, these indices were obviously decreased, suggesting that MSC-EVs relieve DKD-induced renal dysfunction (Fig. 2B, C). Pathologically, glomerular hypertrophy, the mesangial matrix and the thickness of the glomerular basement membrane were significantly increased in the kidneys of DKD mice and were obviously reduced after treatment with MSC-EVs (Fig. 2D, E). Immunohistochemical staining revealed that MSC-EV treatment reduced the number of PCNA-positive cells (Fig. 2F, G). Western blot analysis revealed a similar trend (Figure S1B, C). In addition, MSC-EV treatment notably decreased collagen deposition in the kidney glomeruli of DKD mice (Fig. 2H, I). Moreover, immunofluorescence staining revealed that MSC-EV treatment inhibited the expression of α-SMA, fibronectin and collagen IV in the kidney glomeruli of DKD mice (Fig. 2J, K). Therefore, MSC-EV treatment attenuated renal pathological changes and alleviated fibrosis in DKD model mice.

Given the role of dysregulated autophagy in the pathogenesis of DKD, we investigated whether the protective effect of MSC-EVs on DKD kidneys is related to autophagy. Western blot analysis was performed to measure the levels of autophagy-related molecules. The results revealed that the ratio of LC3II/I was dramatically decreased and that the p62 level was dramatically increased in the kidneys of DKD mice. These effects were reversed by MSC-EV treatment (Fig. 2L, M), indicating that autophagy, which was suppressed in the kidneys of DKD mice, was promoted by MSC-EVs. Taken together, these data demonstrated that MSC-EVs promoted the activation of autophagy and alleviated renal injury and fibrosis induced by DKD.

MSC-EVs inhibited HG-induced mesangial cell proliferation and ECM accumulation and promoted autophagy

Glomerular mesangial expansion due to the proliferation and excessive ECM production of mesangial cells is a key feature of DKD. To identify the role of MSC-EVs in glomerular mesangial cells in DKD, mMCs were induced with HG and treated with MSC-EVs. The results of the CCK-8 assay suggested that cell viability was markedly increased in HG-induced mMCs, but MSC-EV treatment reduced cell viability in HG-induced mMCs

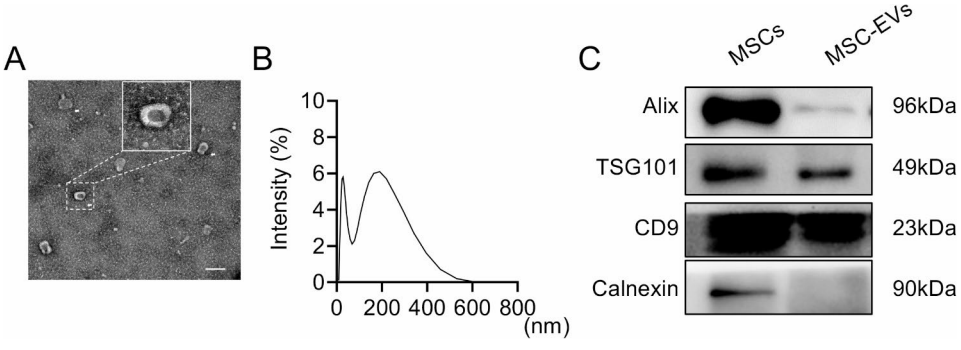

Fig. 1 Characteristics of MSC-EVs. (**A**) The morphology of MSC-EVs was analyzed via transmission electron microscopy (TEM). Scale bar, 100 μm. (**B**) The size distribution of MSC-EVs was measured via dynamic light scattering (DLS). (**C**) Western blot analysis was performed to detect the expression of the EV-associated markers Alix, TSG101, and CD9 and the EV-negative marker calnexin in MSC-EVs. The full-length blots are presented in Supplementary Fig. 5

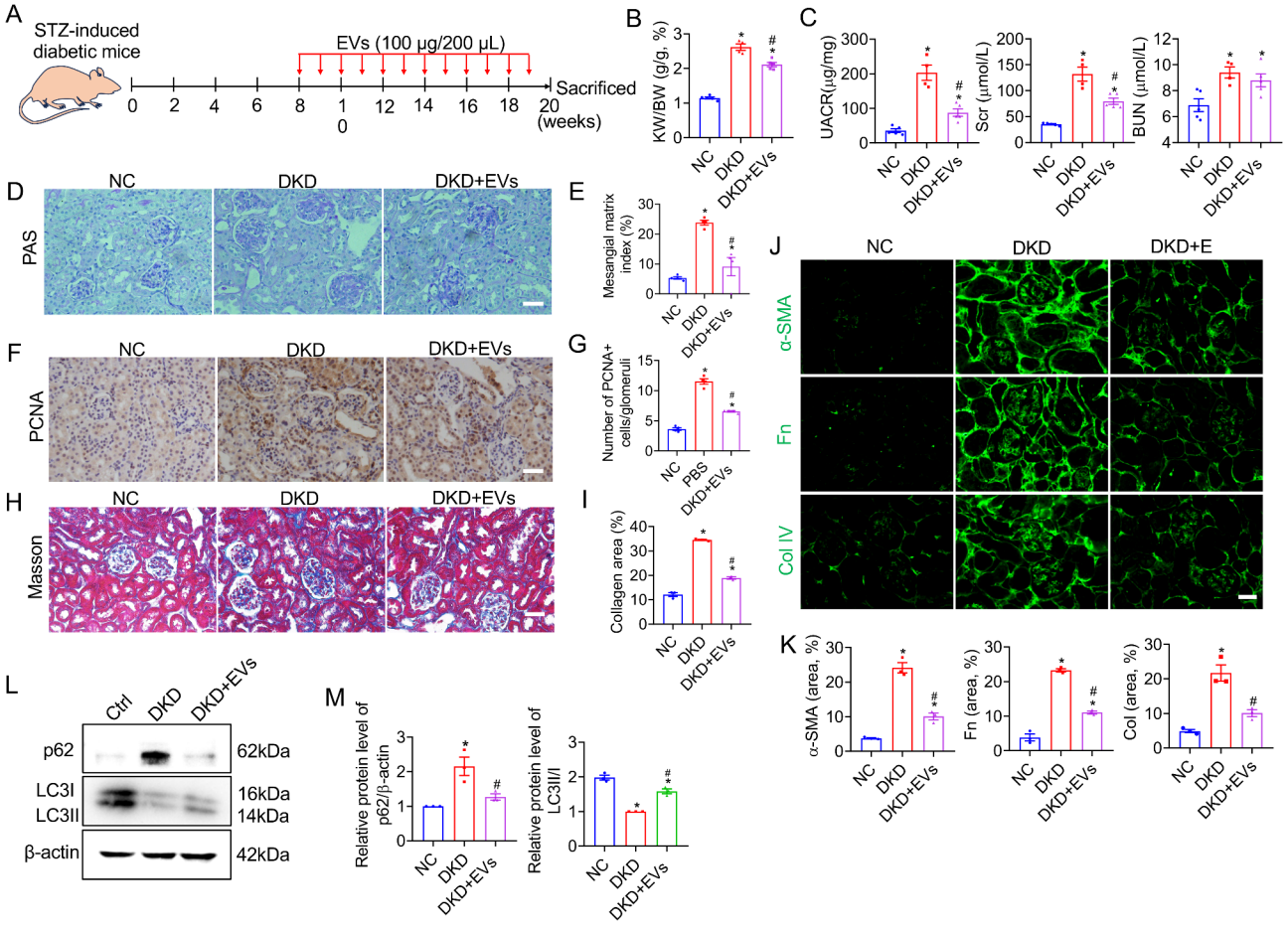

Fig. 2 MSC-EVs ameliorated renal injury and fibrosis and promoted autophagy in STZ-induced DKD mice. (**A**) Schematic diagram of the animal experimental procedures. The mice were intraperitoneally administered 55 mg/kg STZ to induce a diabetic model. After 8 weeks, EVs derived from hP-MSCs (100 μg/200 μL) were administered via the tail vein for 12 weeks. (**B**) Relative kidney weights of the mice. $n = 4$ or 5. (**C**) Renal function of the mice was evaluated by detecting the urinary albumin-to-creatinine ratio (UACR), serum creatinine (Scr), and blood urea nitrogen (BUN). $n = 4$ or 5 (**D**, **E**) Representative images of periodic acid Schiff (PAS) staining and quantification of the mesangial matrix index in mouse kidneys. $n = 4$. Scale bar, 100 μm. (**F**, **G**) Immunohistochemical staining of PCNA in renal sections. The number of PCNA-positive cells in each glomerulus was measured. $n = 4$. Scale bar, 100 μm. (**H**, **I**) Representative images of Masson's trichrome-stained mouse renal sections. The percentage of collagen area in each glomerulus was quantified. $n = 3$. Scale bar, 100 μm. (**J**, **K**) Immunofluorescence staining of α-SMA, fibronectin and Col IV (green) in mouse renal sections. The percentages of α-SMA-, fibronectin- and Col IV-positive areas in each glomerulus were quantified. $n = 3$. Scale bar, 100 μm. (**L**, **M**) Representative western blot images and quantification of the expression of LC3II/LC3I and p62 in the renal cortex of a mouse. β-actin was used as a loading control. The full-length blots are presented in Supplementary Fig. 6; $n = 3$. The data are expressed as the means ± SEMs. Statistical analysis was performed via one-way ANOVA with Tukey's multiple comparison tests. $^{*}P < 0.05$ versus NC; $^{\#}p < 0.05$ versus DKD. Abbreviations: STZ, streptavidin. Fn, fibronectin. Col IV, Collagen IV. PCNA, Proliferating Cell Nuclear Antigen

(Fig. 3A). Moreover, western blot analysis revealed that the expression of PCNA was obviously increased in HG-induced mMCs but was suppressed by MSC-EV treatment (Fig. 3B, C). In addition, an EdU assay revealed that the percentage of EdU-positive cells in HG-induced mMCs was markedly increased, whereas MSC-EV treatment reduced the percentage of EdU-positive cells in HG-induced mMCs, suggesting that MSC-EVs inhibited HG-induced proliferation of mMCs (Fig. 3D, E). Then, immunofluorescence staining and RT–qPCR were used to measure fibrosis-related indicators. The results demonstrated that the expression of α-SMA, fibronectin and collagen IV in HG-induced mMCs was significantly upregulated, and MSC-EV treatment downregulated the expression of these indicators in HG-induced mMCs, demonstrating that MSC-EVs inhibited ECM accumulation in HG-induced mMCs (Fig. 3F, G, Figure S2).

Next, we investigated whether MSC-EVs affect autophagy in mesangial cells. Western blot analysis revealed that the expression of LC3II/I was dramatically decreased and that the expression of p62 was dramatically increased in HG-induced mMCs. These effects were reversed by MSC-EV treatment (Fig. 3H, I). Collectively, these data indicate that MSC-EV treatment promoted autophagy and inhibited cell proliferation and ECM accumulation in HG-induced mesangial cells.

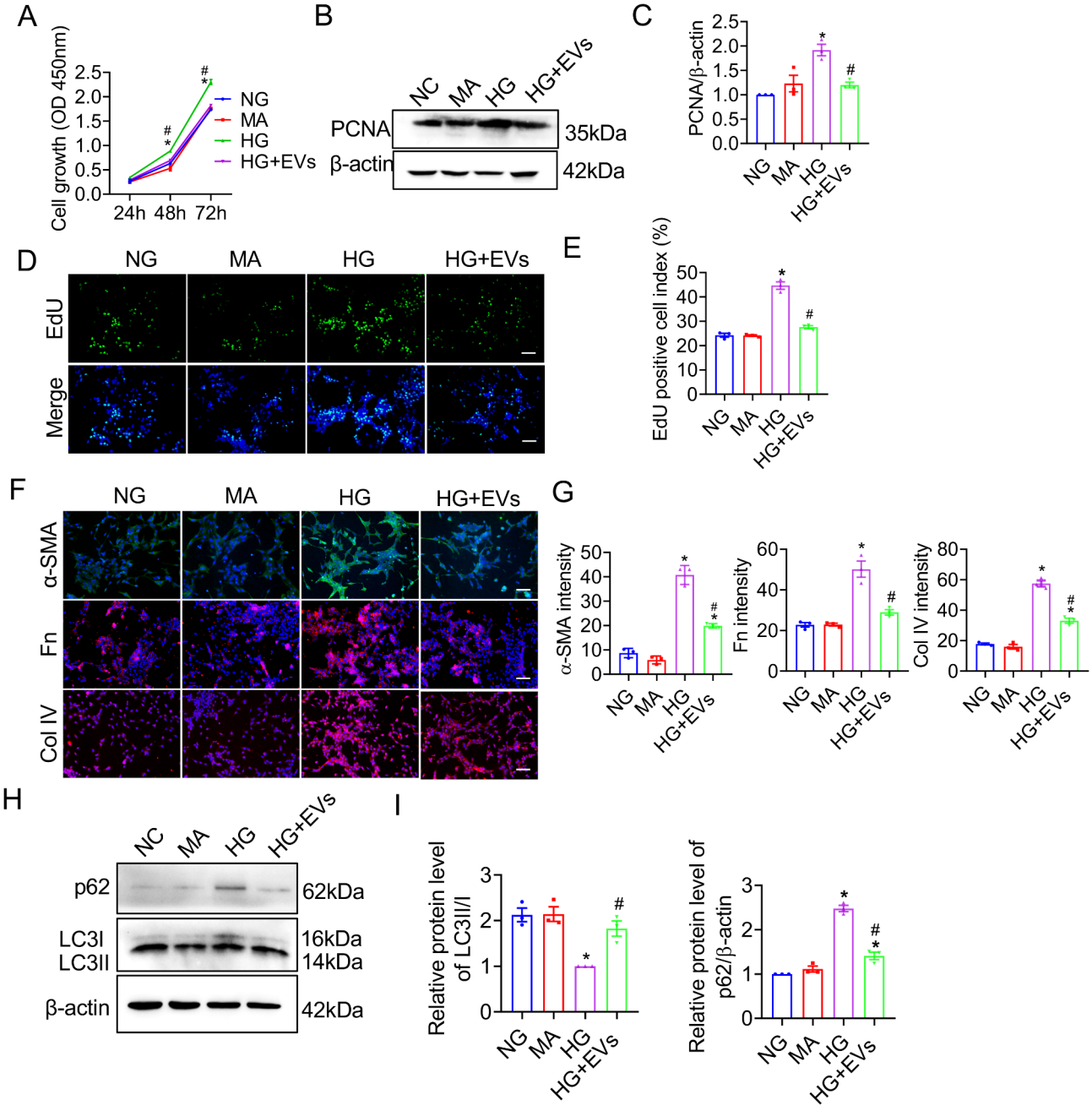

Fig. 3 MSC-EVs inhibited mMC proliferation and ECM accumulation and promoted autophagy. (**A**) Cell viability of mMCs was measured by a CCK-8 assay under conditions of NG, M, HG or HG plus MSC-EVs for 24, 48 and 72 h. (**B**, **C**) Representative western blot images and quantitative analysis of PCNA expression in mMCs. β-actin was used as a loading control. The full-length blots are presented in Supplementary Fig. 7. (**D**, **E**) EdU incorporation assay in mMCs subjected to different treatments and quantification of the number of EdU-positive cell nuclei (green)/total number of cell nuclei (blue). Nuclei were counterstained with Hoechst 33,342. Scale bar, 100 μm. (**F**, **G**) Immunofluorescence staining and quantification of α-SMA (green), fibronectin (red) and Col IV (red) expression in mMCs subjected to different treatments. Nuclei (blue) were counterstained with DAPI. Scale bar, 100 μm. (**H**, **I**) Representative western blot images and quantitative analysis of LC3II/LC3I and p62 expression in mMCs. β-actin was used as a loading control. The full-length blots are presented in Supplementary Fig. 7; $n = 3$. The data are expressed as the means ± SEMs. Statistical analysis was performed via one-way ANOVA with Tukey's multiple comparison tests. $^{*}P < 0.05$ versus NG; $^{\#}p < 0.05$ versus HG. Abbreviations: NG, normal glucose. MA, mannitol. HG, high glucose. PCNA, Proliferating Cell Nuclear Antigen. Fn, fibronectin. Col IV, Collagen IV

miR-99b-5p-enriched MSC-EVs inhibited the expression of mTOR

To determine the underlying mechanisms by which MSC-EVs mediate autophagy, we performed further studies. Zhang et al. identified the top 37 miRNAs in EVs derived from hP-MSCs, of which the fifth most abundant miRNA, miR-99b-5p, was the molecule of interest [3]. The miRNA–gene relationship prediction websites TargetScan, mirDIP, and miRDB predicted that miR-99b-5p participated in the regulation of mTOR, a critical regulator of autophagy (Fig. 4A). Bioinformatics analysis revealed that mTOR was a target of miR-99b-5p (Fig. 4B). To confirm the internalization of miR-99b-5-enriched MSC-EVs by mMCs, Dil-EVs or EVs were incubated with mMCs. Fluorescence microscopy and RT–qPCR revealed that MSC-EVs were internalized by mMCs and that miR-99b-5p expression was upregulated in mMCs, whereas *mTOR* expression was downregulated (Fig. 4C, D). To confirm the role of miR-99b-5p in MSC-EV-mediated mTOR inhibition, hP-MSCs were transfected with an inhibitor-negative control or a miR-99b-5p inhibitor. Inhibitor-negative control MSC-EVs (EVs-NC) and miR-99b-5p-knockdown MSC-EVs (EVs-KD) were isolated from the supernatant of hP-MSCs. RT–qPCR analysis confirmed the decreased expression of miR-99b-5p in the EV-KD group compared with the EV-NC group (Fig. 4E). Then, the mMCs were incubated with EVs-NC or EVs-KD for 24 h, and western blot analysis demonstrated that miR-99b-5p downregulated the expression of mTOR (Fig. 4F). In summary, these results suggested that miR-99b-5p delivered by MSC-EVs directly targeted the *mTOR* gene.

miR-99b-5p delivered by MSC-EVs inhibited proliferation and ECM accumulation in HG-induced GMCs via mTOR-mediated autophagy

Next, we investigated the effects of miR-99b-5p in MSC-EVs on the proliferation and ECM synthesis of HG-induced mMCs. A CCK-8 assay revealed that, under HG conditions, treatment with EVs-NC markedly suppressed the viability of mMCs, whereas EV-KD treatment increased the viability of mMCs (Fig. 5A). Western blot analysis revealed that EV-NC treatment obviously decreased the expression of PCNA in HG-induced mMCs, whereas EV-KD treatment reversed this effect (Fig. 5B, C). In addition, an EdU assay revealed that the percentage of EdU-positive cells was markedly decreased in HG-induced mMCs treated with EVs-NC, which was reversed by EVs-KD (Fig. 5D, E), indicating that delivery of miR-99b-5p into mMCs via MSC-EVs inhibited HG-induced cell proliferation. Then, immunofluorescence staining and RT–qPCR were used to measure the expression of fibrosis-related indicators in HG-induced mMCs. The results demonstrated that treatment with EVs-NC significantly downregulated the expression of α-SMA, fibronectin and collagen IV in HG-induced mMCs. In

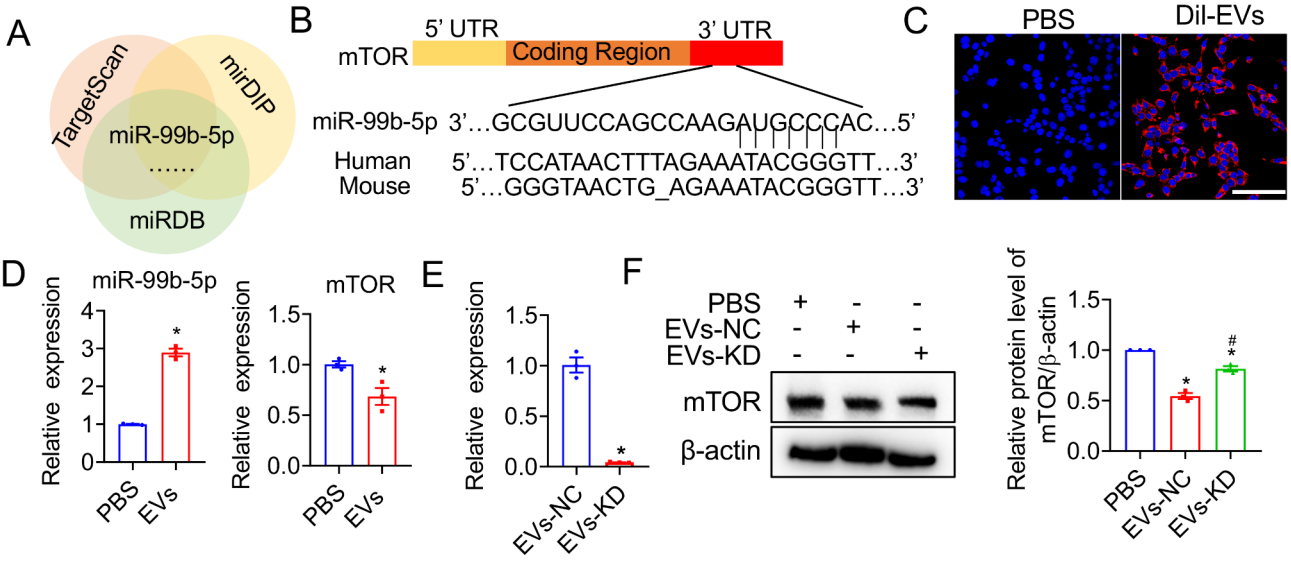

Fig. 4 mTOR was the target of miR-99b-5p transferred by MSC-EVs. (**A**) Bioinformatics analysis was performed via the TargetScan, mirDIP and miRDB databases to predict potential interactions between mTOR and miR-99b-5p. (**B**) Scheme of the putative binding sites between the 3′ UTR of mTOR mRNA and miR-99b-5p. (**C**, **D**) The relative expression of miR-99b-5p and *mTOR* in mMCs incubated with MSC-EVs for 24 h was detected by RT–qPCR. $n = 3$. $^{*}P < 0.05$ versus PBS. (**E**) The relative expression of miR-99b-5p in the miR-99b-5p inhibitor-stimulated MSC-EVs was assessed via RT–qPCR. $n = 3$. $^{*}P < 0.05$ versus EVs-NC. (**F**, **G**) Western blot analysis and quantification of mTOR and p-mTOR expression in mMCs treated with EV-NC or EV-KD for 24 h. β-actin was used as a loading control. The full-length blots are presented in Supplementary Fig. 8; $n = 3$. $^{*}P < 0.05$ versus PBS; $^{\#}p < 0.05$ versus EV-KD. The data are expressed as the means ± SEMs. For (**C**, **D and E**), statistical analysis was performed via a two-tailed unpaired Student's *t* test. For (**F**), statistical analysis was performed via one-way ANOVA with Tukey's multiple comparison test

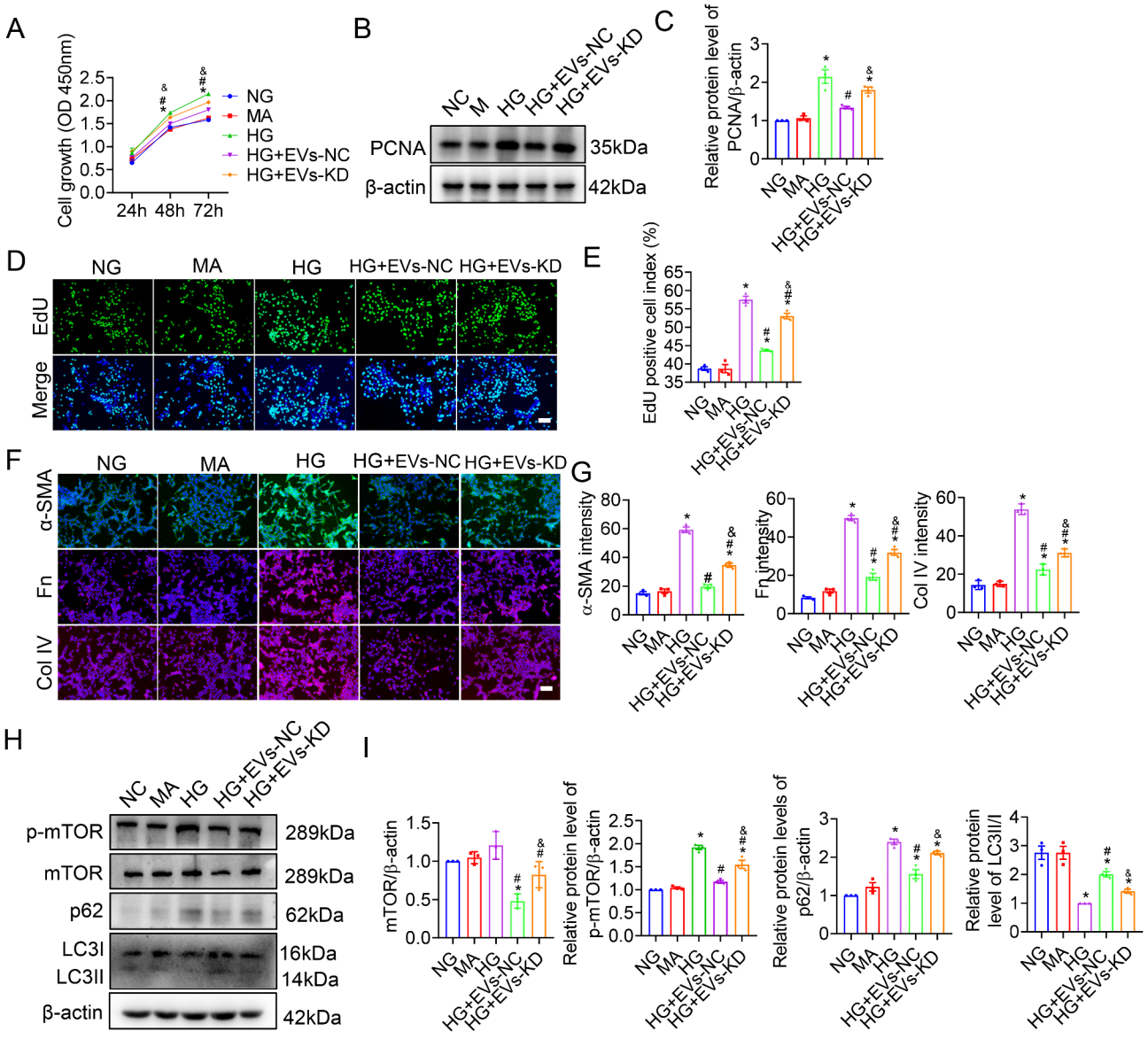

Fig. 5 miR-99b-5p delivered by MSC-EVs inhibited HG-induced proliferation and ECM accumulation by promoting mTOR-mediated autophagy in mMCs. (**A**) Cell viability of mMCs was measured by a CCK-8 assay under conditions of NG, MA, HG, and HG with EVs-NC or HG with EVs-KD for 24, 48 and 72 h. (**B**, **C**) Representative Western blot images and quantitative analysis of PCNA expression in mMCs subjected to different treatments. β-actin was used as a loading control. The full-length blots are presented in Supplementary Fig. 9. (**D**, **E**) EdU incorporation assay in mMCs subjected to different treatments and quantification of the number of EdU-positive cell nuclei (green)/total number of cell nuclei (blue). Nuclei were counterstained with Hoechst 33,342. Scale bar, 100 μm. (**F**, **G**) Immunofluorescence staining and quantification of α-SMA (green), fibronectin (red) and Col IV (red) expression in mMCs subjected to different treatments. Nuclei (blue) were counterstained with DAPI. Scale bar, 100 μm. (**H**, **I**) Representative western blot images and quantitative analysis of mTOR, p-mTOR, LC3II/LC3I and p62 expression in mMCs subjected to different treatments. β-actin was used as a loading control. The full-length blots are presented in Supplementary Fig. 9; $n = 3$. The data are expressed as the means ± SEMs. Statistical analysis was performed via one-way ANOVA with Tukey's multiple comparison tests. $^{*}P < 0.05$ versus NG; $^{\#}p < 0.05$ versus HG. $^{\&}p < 0.05$ versus HG + EV-NC. Abbreviations: NG, normal glucose. HG, high glucose

contrast, EV-KD resulted in increased expression of these indicators (Fig. 5F, G, Figure S3), demonstrating that the transfer of miR-99b-5p by MSC-EVs suppressed HG-induced ECM accumulation in mMCs.

We subsequently investigated the role of miR-99b-5p delivered by MSC-EVs in the protection of HG-induced mMCs via mTOR-mediated autophagy. Western blotting analysis revealed that treatment with EVs-NC led to significantly downregulated expression of mTOR, p-mTOR and p62 accompanied by increased expression of LC3II/I in HG-induced mMCs, whereas EV-KD obviously elevated the expression of mTOR, p-mTOR and p62 accompanied by reduced expression of LC3II/I (Fig. 5H, I). These data suggest that miR-99b-5p delivered by MSC-EVs inhibits mTOR expression, resulting

in the promotion of autophagy and the inhibition of HG-induced mMC injury.

miR-99b-5p delivered by MSC-EVs ameliorated renal injury and fibrosis via mTOR-mediated autophagy in STZ-induced diabetic mice

To investigate the effects of miR-99b-5p transferred by MSC-EVs in DKD, EVs-NC or EVs-KD were administered intravenously into STZ-induced diabetic mice. Functionally, the results revealed that EV-NC treatment obviously reduced the levels of proteinuria, serum creatinine and blood urea nitrogen in DKD mice, whereas EV-KD markedly increased the levels of proteinuria, serum creatinine and blood urea nitrogen (Fig. 6A). Pathologically, PAS staining revealed that glomerular hypertrophy, the mesangial matrix and the thickness of the glomerular basement membrane were significantly alleviated in the kidneys of DKD mice treated with EV-NC, and EV-KD aggravated these histopathological changes (Fig. 6B, C). Immunohistochemical staining revealed that EV-NC treatment reduced the number of PCNA-positive cells in the kidney glomeruli of DKD mice, and these effects were reversed by EV-KD treatment (Fig. 6D, E), which was confirmed by Western blot analysis (Figure S4). In addition, EV-NC treatment notably decreased collagen deposition in the kidney glomeruli of DKD mice, and EV-KD treatment resulted in increased collagen deposition (Fig. 6F, G). Moreover, immunofluorescence staining revealed that EV-NC treatment inhibited the expression of α-SMA, fibronectin and collagen IV in the kidney glomeruli of DKD mice, and these effects were reversed by EV-KD treatment (Fig. 6H, I). Therefore, delivery of miR-99b-5p via MSC-EVs attenuated renal injury and alleviated fibrosis in DKD model mice.

Western blot analysis was used to investigate the role of miR-99b-5p delivered by MSC-EVs in the renoprotection of DKD via mTOR-mediated autophagy. The results demonstrated that treatment with EVs-NC led to significantly downregulated expression of mTOR and p-mTOR accompanied by increased expression of LC3II/I in the kidneys of DKD mice, whereas EV-KD treatment obviously elevated the expression of mTOR, p-mTOR and p62 accompanied by reduced expression of LC3II/I (Fig. 6J, K). These data suggest that the delivery of miR-99b-5p by MSC-EVs inhibits mTOR expression, resulting in the promotion of autophagy and the inhibition of DKD-induced renal injury.

Discussion

DKD is a severe complication of diabetes mellitus and is characterized by progressive ECM accumulation in the glomerular mesangium and basement membrane thickening, ultimately leading to glomerulosclerosis. Mesangial cells, as key intrinsic components of the glomerulus, undergo aberrant alterations that contribute to mesangial expansion and glomerulosclerosis, driving DKD progression. Recently, MSC-EVs have emerged as promising therapeutics for DKD. In this study, we investigated the therapeutic effects and underlying mechanisms of MSC-EVs in DKD. Our findings demonstrated that MSC-EVs attenuate kidney damage and fibrosis by inhibiting cell proliferation and ECM accumulation in glomerular mesangial cells. Mechanistically, MSC-EVs delivered miR-99b-5p, which enhanced autophagy by suppressing *mTOR* expression. This process inhibited both cell proliferation and ECM accumulation in high glucose (HG)-induced mesangial cells. In summary, our study revealed that MSC-EVs mitigate diabetic kidney injury and fibrosis by promoting mTOR-mediated autophagy through the transfer of miR-99b-5p (Fig. 7).

MSC-EVs have been demonstrated to have effective therapeutic effects on DKD through various pathways, including antiapoptotic, anti-inflammatory, antifibrotic, and antioxidative mechanisms, as well as through the enhancement of autophagy [36]. These effects are mediated by the transfer of genetic materials and proteins. For example, EVs derived from human umbilical cord MSCs enriched with miR-424-5p have been shown to protect renal tubular epithelial cells from apoptosis and epithelial–mesenchymal transition (EMT) by inhibiting YAP1 activity [29]. In addition, small EVs derived from MSCs promoted the ubiquitination of YAP in mesangial cells and attenuated renal interstitial fibrosis to alleviate DKD progression by delivering CK1δ/β-TRCP [37]. Another study indicated that miR-22-3p delivered by human umbilical cord MSC-derived EVs targeted the NLRP3 inflammasome to protect podocytes and diabetic mice from inflammation [28]. In this study, we found that miR-99b-5p-enriched hP-MSC-derived EVs restrained the proliferation and ECM accumulation of glomerular mesangial cells in DKD by promoting autophagy. Moreover, studies have revealed that MSC-EVs have therapeutic effects on diabetes mellitus (DM) and other diabetic complications. In addition, human umbilical cord MSC-derived EVs improved β-cell function in T2DM mice via the inhibition of NRF2-mediated ferroptosis through the AKT/ERK signaling pathway [38]. Mouse bone MSC-derived EVs ameliorate diabetes-induced cardiomyopathy by reducing TAK1-pJNK-NFKB inflammation-associated expression and cardiac hypertrophy and fibrosis [39]. Thus, MSC-EVs may be a potential therapeutic modality for DM and diabetic complications, and the clinical application of MSC-EVs is being explored. However, further research should be conducted to address the challenges associated with the translational application of MSC-EVs, including the complex pathogenesis of DKD, the therapeutic efficacy of MSC-EVs for patients with DKD, and the preparation and quality control of MSC-EVs [40].

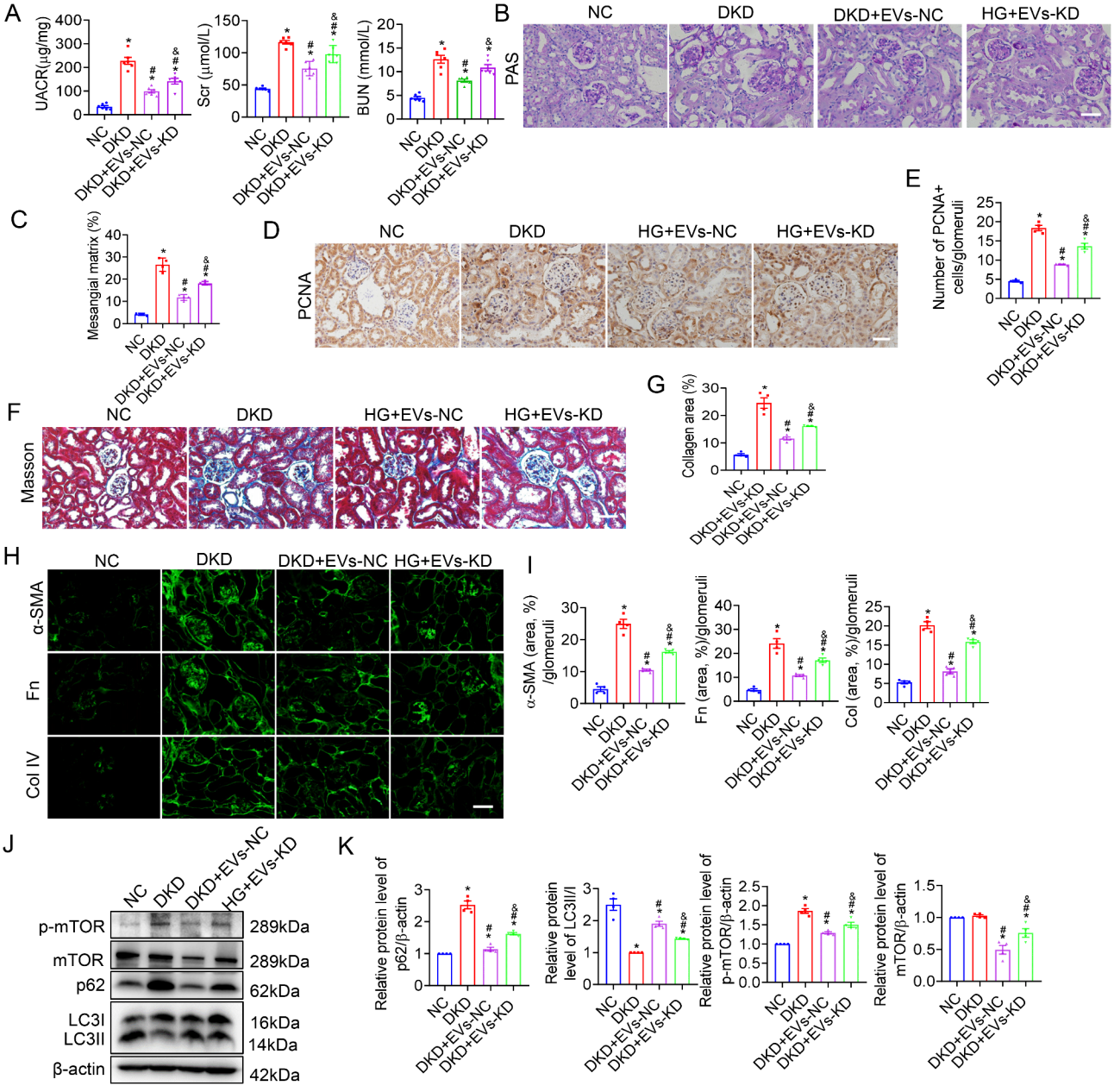

Fig. 6 miR-99b-5p delivered by MSC-EVs ameliorated renal injury in STZ-induced DKD mice by promoting mTOR-mediated autophagy. (**A**) Renal function of the mice was evaluated by detecting the urinary albumin-to-creatinine ratio (UACR), serum creatinine (Scr), and blood urea nitrogen (BUN). $n = 6$. (**B**, **C**) Representative images of periodic acid–Schiff (PAS) staining and quantification of the mesangial matrix index in mouse kidneys. $n = 4$. Scale bar, 100 μm. (**D**, **E**) The percentage of PCNA-positive cells in the kidney glomeruli of the mice was quantified via immunohistochemical staining. $n = 4$. (**F**, **G**) Representative images of Masson staining of mouse kidney sections and quantification of the collagen deposition area in the glomerulus. Scale bar, 100 μm. (**H**, **I**) Immunofluorescence staining and quantification of α-SMA, fibronectin and Col IV (green) expression in kidney sections. $n = 4$. Scale bar, 100 μm. (**J**, **K**) Representative western blot images and quantification showing the expression of mTOR, p-mTOR, LC3II/LC3I and p62 in the renal cortex of mice. β-actin was used as a loading control. The full-length blots are presented in Supplementary Fig. 10; $n = 4$. The data are expressed as the means ± SEMs. Statistical analysis was performed via one-way ANOVA with Tukey's multiple comparison tests. $^{*}P < 0.05$ versus NC; $^{\#}p < 0.05$ versus DKD. $^{\&}p < 0.05$ versus DKD + EVs-NC. Abbreviations: STZ, streptavidin. Fn, fibronectin. Col IV, Collagen IV. PCNA, Proliferating Cell Nuclear Antigen

MicroRNAs (miRNAs) are small noncoding RNAs that degrade or repress the translation of target mRNAs to silence gene expression. Many studies have shown the critical role of microRNAs in DKD pathogenesis [41]. For example, exosomal miR-92a-1-5p released by proximal tubular epithelial cells induced endoplasmic reticulum stress and epithelial–mesenchymal transition in mouse mesangial cells through reticulocabin-3 modulation in DKD [42]. MiR-99b-5p contributes to a variety of biological processes, including proliferation,

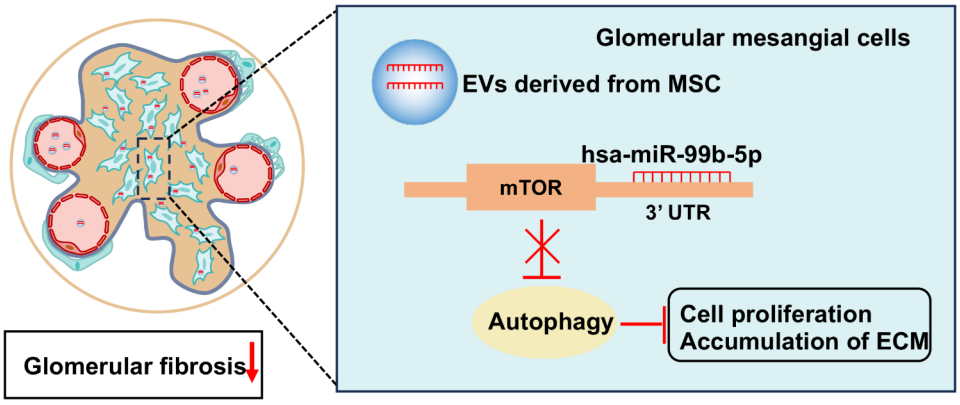

Fig. 7 Graphical summary of MSC-EV-based DKD therapy. EVs derived from hP-MSCs alleviated DKD-induced renal injury and glomerular fibrosis. miR-99b-5p transferred by MSC-EVs targets and inhibits mTOR, promoting autophagy, which relieves the proliferation and ECM accumulation of glomerular mesangial cells

invasion, metastasis, irradiation resistance and neuroinflammation. Aberrant regulation of miR-99b-5p has been demonstrated in various cancers and tissue damage [43, 44]. The results of miRNA sequencing revealed that the expression of miR-99b-5p is high in EVs derived from hP-MSCs [3]. In the present study, our data indicated that miR-99b-5p delivered by MSC-EVs obviously improved DKD-induced renal injury and fibrosis by repressing the proliferation and accumulation of ECM in mesangial cells, indicating a therapeutic function of miR-99b-5p in DKD. Convincing evidence shows that miR-99b-5p is involved in diabetic complications [45, 46]. For example, abnormal expression of miR-99b-5p has been observed in diabetic neuropathy, and miR-99b-5p in EVs derived from bone marrow MSCs promoted the growth and angiogenesis of HG-treated HUVECs to improve diabetic wounds [45, 46].

Progressive deposition of the ECM in the glomerular mesangium and hyperplasia in glomerular mesangial cells are the landmarks of DKD. Autophagy can inhibit mesangial cell activation and epithelial–mesenchymal transition in renal tubular epithelial cells to alleviate renal glomerular fibrosis and tubulointerstitial fibrosis in DKD [47, 48]. In line with these observations, we found that MSC-EVs promoted autophagy in both HG-stimulated mMCs and the kidneys of DKD model mice, relieving DKD-induced renal injury. mTOR, a conserved protein kinase in all species, is hyperactivated in the diabetic kidney to accelerate kidney injury [49]. Suppression of mTOR by rapamycin, an inhibitor of mTOR, ameliorated morphological disorders and renal dysfunctions in diabetic animal models [50, 51]. Furthermore, accumulating evidence has demonstrated that mTOR acts as the master negative regulator of autophagy in DKD [12, 18]. The present study revealed that the phosphorylation of mTOR was induced in mMCs and kidneys under diabetic conditions, with the suppression of autophagy. MSC-EV treatment markedly inhibited the expression and activity of mTOR, promoting autophagy, which was reversed by miR-99b-5p knockdown. Therefore, miR-99b-5p transferred by MSC-EVs into mMCs targets mTOR, thereby promoting autophagy to alleviate HG-induced proliferation and ECM accumulation in mMCs.

However, the limitations of the present study were that we did not identify the possible influence of other cargos in MSC-EVs on DKD. Therefore, further studies should be conducted to explore the exact mechanism by which MSC-EVs improve DKD. The efficacy of EVs is determined mainly by their cargo, targeting, and route of administration. Exogenously injected MSC-EVs can be successfully engrafted into the kidneys of DKD mice, but a large proportion of MSC-EVs accumulate in the liver [52]. Thus, novel strategies to increase the kidney-targeting ability of MSC-EVs are urgently needed. Moreover, whether the inhibition of tubulointerstitial fibrosis is associated with the autophagy activation induced by MSC-EVs and the underlying mechanism of action need to be verified in our future studies.

Conclusions

In conclusion, our study demonstrated that EVs derived from hP-MSCs could effectively protect against the progression of DKD. miR-99b-5p carried by MSC-EVs inhibits proliferation and ECM accumulation in glomerular mesangial cells by regulating mTOR-mediated autophagy under diabetic conditions. Our findings suggest that EVs derived from hP-MSCs may constitute a promising cell-free therapeutic strategy for patients with DKD in the future.

Abbreviations

BUN	Blood Urea Nitrogen
CCK-8	Cell Counting Kit-8
Cr	Creatinine; DKD: Diabetic Kidney Disease
DKD	Diabetic Kidney Disease

DLS	Dynamic Light Scattering
EdU	5-ethynyl-2′-deoxyuridine
ELISA	Enzyme-Linked Immunosorbent Assay
EMT	Epithelial-to-Mesenchymal Transition
ESRD	End-Stage Renal Disease
EVs	Extracellular Vesicles
hP-MSCs	Human Placental Mesenchymal Stem Cells
mMCs	Mouse Glomerular Mesangial Cells
mTOR	Mechanistic Target of Rapamycin
PAS	Periodic Acid Schiff
PCNA	Proliferating Cell Nuclear Antigen
STZ	Streptozotocin
α-SMA	Alpha Smooth Muscle Actin

Supplementary Information

The online version contains supplementary material available at https://doi.org/10.1186/s13287-025-04265-x.

Supplementary Material 1

Acknowledgements
The authors declare that they have not used AI-generated work in this manuscript.

Author contributions
RRL & HT performed all the experiments. KP, RL, and ZG contributed to the molecular imaging, manuscript review and editing. ZL & XC contributed to the study conception, design, and financial support. All the authors were involved in the final approval of the manuscript.

Funding
This study was financially supported by the National Natural Science Foundation of China (82472169), the Tianjin Natural Science Foundation (22JCZXJC00170), and the Open funding from the Nankai University Eye Institute (NKYKD202203).

Data availability
All data are included in the article and its Supplementary Information files or are available from the corresponding authors upon reasonable request.

Declarations

Ethics approval and consent to participate
The Ethics Committee for the Use of Animals of Nankai University approved the experimental protocols for studies of mesenchymal stem cells (MSCs) for kidney injury therapy (project title: Therapeutic effects and mechanisms of mesenchymal stem cells (MSCs) for acute and chronic injury; Approval no. 20210051; Date of approval: May 20, 2021). Human placenta-derived mesenchymal stem cells (hP-MSCs) were purchased from AmCellGene Co. Ltd., Tianjin, China (https://www.amcellgene.com/). AmCellGene Co. Ltd. confirmed that there was initial ethical approval for collection of hP-MSCs, and the donors had signed informed consent.

Consent for publication
Not applicable.

Competing interests
The authors declare that they have no competing interests.

Received: 11 December 2024 / Accepted: 4 March 2025
Published online: 18 March 2025

References

1. Gupta S, Dominguez M, Golestaneh L. Diabetic kidney disease: an update. Med Clin North Am. 2023;107(4):689–705. https://doi.org/10.1016/j.mcna.2023.03.004.
2. Zhang Q, Sun T, Yu F, Liu W, Gao J, Chen J, et al. PAFAH2 suppresses synchronized ferroptosis to ameliorate acute kidney injury. Nat Chem Biol. 2024;20(7):835–46. https://doi.org/10.1038/s41589-023-01528-7.
3. Zhang K, Li R, Chen X, Yan H, Li H, Zhao X, et al. Renal endothelial Cell-Targeted extracellular vesicles protect the kidney from ischemic injury. Adv Sci (Weinh). 2023;10(3):e2204626. https://doi.org/10.1002/advs.202204626.
4. Thomas MC, Brownlee M, Susztak K, Sharma K, Jandeleit-Dahm KAM, Zoungas S, et al. Diabetic kidney disease. Nat Reviews Disease Primers. 2015;1(1):15018. https://doi.org/10.1038/nrdp.2015.18.
5. Avraham S, Korin B, Chung J-J, Oxburgh L, Shaw AS. The mesangial cell — the glomerular stromal cell. Nat Rev Nephrol. 2021;17(12):855–64. https://doi.org/10.1038/s41581-021-00474-8.
6. Hu S, Hang X, Wei Y, Wang H, Zhang L, Zhao L. Crosstalk among podocytes, glomerular endothelial cells and mesangial cells in diabetic kidney disease: an updated review. Cell Commun Signal. 2024;22(1):136. https://doi.org/10.1186/s12964-024-01502-3.
7. Guo W, Li H, Li Y, Kong W. Renal intrinsic cells remodeling in diabetic kidney disease and the regulatory effects of SGLT2 inhibitors. Biomed Pharmacother. 2023;165:115025. https://doi.org/10.1016/j.biopha.2023.115025.
8. Zhang C, Shang Y, Chen X, Midgley AC, Wang Z, Zhu D, et al. Supramolecular nanofibers containing Arginine-Glycine-Aspartate (RGD) peptides boost therapeutic efficacy of extracellular vesicles in kidney repair. ACS Nano. 2020;14(9):12133–47. https://doi.org/10.1021/acsnano.0c05681.
9. Salemkour Y, Yildiz D, Dionet L, t, Hart DC, Verheijden KAT, Saito R et al. (2023). Podocyte Injury in Diabetic Kidney Disease in Mouse Models Involves TRPC6-mediated Calpain Activation Impairing Autophagy. *J Am Soc Nephrol, 34*(11), 1823–1842. https://doi.org/10.1681/asn.0000000000000212
10. Ma Z, Li L, Livingston MJ, Zhang D, Mi Q, Zhang M, et al. p53/microRNA-214/ULK1 axis impairs renal tubular autophagy in diabetic kidney disease. J Clin Invest. 2020;130(9):5011–26. https://doi.org/10.1172/jci135536.
11. Lenoir O, Jasiek M, Hénique C, Guyonnet L, Hartleben B, Bork T, et al. Endothelial cell and podocyte autophagy synergistically protect from diabetes-induced glomerulosclerosis. Autophagy. 2015;11(7):1130–45. https://doi.org/10.1080/15548627.2015.1049799.
12. Chen K, Yu B, Liao J. LncRNA SOX2OT alleviates mesangial cell proliferation and fibrosis in diabetic nephropathy via Akt/mTOR-mediated autophagy. Mol Med. 2021;27(1):71. https://doi.org/10.1186/s10020-021-00310-6.
13. Tang C, Livingston MJ, Liu Z, Dong Z. Autophagy in kidney homeostasis and disease. Nat Rev Nephrol. 2020;16(9):489–508. https://doi.org/10.1038/s41581-020-0309-2.
14. Liu L, Yang L, Chang B, Zhang J, Guo Y, Yang X. The protective effects of Rapamycin on cell autophagy in the renal tissues of rats with diabetic nephropathy via mTOR-S6K1-LC3II signaling pathway. Ren Fail. 2018;40(1):492–7. https://doi.org/10.1080/0886022x.2018.1489287.
15. Li XY, Wang SS, Han Z, Han F, Chang YP, Yang Y, et al. Triptolide restores autophagy to alleviate diabetic renal fibrosis through the miR-141-3p/PTEN/Akt/mTOR pathway. Mol Ther Nucleic Acids. 2017;9:48–56. https://doi.org/10.1016/j.omtn.2017.08.011.
16. Dong R, Zhang X, Liu Y, Zhao T, Sun Z, Liu P, et al. Rutin alleviates EndMT by restoring autophagy through inhibiting HDAC1 via PI3K/AKT/mTOR pathway in diabetic kidney disease. Phytomedicine. 2023;112:154700. https://doi.org/10.1016/j.phymed.2023.154700.
17. Jin J, Shi Y, Gong J, Zhao L, Li Y, He Q, et al. Exosome secreted from adipose-derived stem cells attenuates diabetic nephropathy by promoting autophagy flux and inhibiting apoptosis in podocyte. Stem Cell Res Ther. 2019;10(1):95. https://doi.org/10.1186/s13287-019-1177-1.
18. Yang D, Livingston MJ, Liu Z, Dong G, Zhang M, Chen JK, et al. Autophagy in diabetic kidney disease: regulation, pathological role and therapeutic potential. Cell Mol Life Sci. 2018;75(4):669–88. https://doi.org/10.1007/s00018-017-2639-1.
19. Zhang MZ, Wang Y, Paueksakon P, Harris RC. Epidermal growth factor receptor Inhibition slows progression of diabetic nephropathy in association with a decrease in Endoplasmic reticulum stress and an increase in autophagy. Diabetes. 2014;63(6):2063–72. https://doi.org/10.2337/db13-1279.
20. Yamahara K, Kume S, Koya D, Tanaka Y, Morita Y, Chin-Kanasaki M, et al. Obesity-mediated autophagy insufficiency exacerbates proteinuria-induced tubulointerstitial lesions. J Am Soc Nephrol. 2013;24(11):1769–81. https://doi.org/10.1681/asn.2012111080.
21. Li Z, Han Z, Han Z-C. Mesenchymal stem cells in clinical trials for immune disorders. Global Med Genet. 2024;11(03):196–9. https://doi.org/10.1055/s-0044-1788044.

22. Pan K, Li Q, Guo Z, Li Z. Healing action of Interleukin-4 (IL-4) in acute and chronic inflammatory conditions: mechanisms and therapeutic strategies. Pharmacol Ther. 2025;265:108760. https://doi.org/10.1016/j.pharmthera.2024.108760.
23. Zhu D, Liu S, Huang K, Wang Z, Hu S, Li J, et al. Intrapericardial exosome therapy dampens cardiac injury via activating Foxo3. Circ Res. 2022;131(10):e135–50. https://doi.org/10.1161/circresaha.122.321384.
24. Liu Y, Chen S, Huang HY, Midgley AC, Han ZB, Han ZC, et al. Ligand-Tethered extracellular vesicles mediated RNA therapy for liver fibrosis. Adv Healthc Mater. 2025;14(2):e2403068. https://doi.org/10.1002/adhm.202403068.
25. Popowski KD, López de Juan Abad B, George A, Silkstone D, Belcher E, Chung J, et al. Inhalable exosomes outperform liposomes as mRNA and protein drug carriers to the lung. Extracell Vesicle. 2022;1:100002. https://doi.org/10.1016/j.vesic.2022.100002.
26. Fu E, Li Z. Extracellular vesicles: A new frontier in the theranostics of cardiovascular diseases. iRADIOLOGY. 2024;2(3):240–59. https://doi.org/10.1002/ird3.77.
27. Li R, Wang C, Chen X, Fu E, Zhang K, Tao H et al. (2024). Phosphatidylserine-mediated uptake of extracellular vesicles by hepatocytes ameliorates liver ischemia-reperfusion injury. *Apoptosis*, 2025;30:69–82. https://doi.org/10.1007/s10495-024-02030-8
28. Wang Y, Liu J, Wang H, Lv S, Liu Q, Li S, et al. Mesenchymal stem Cell-Derived exosomes ameliorate diabetic kidney disease through the NLRP3 signaling pathway. Stem Cells. 2023;41(4):368–83. https://doi.org/10.1093/stmcls/sxad010.
29. Cui C, Zang N, Song J, Guo X, He Q, Hu H, et al. Exosomes derived from mesenchymal stem cells attenuate diabetic kidney disease by inhibiting cell apoptosis and epithelial-to-mesenchymal transition via miR-424-5p. Faseb J. 2022;36(10):e22517. https://doi.org/10.1096/fj.202200488R.
30. Huang H, Qian M, Liu Y, Chen S, Li H, Han Z, et al. Genetically engineered mesenchymal stem cells as a nitric oxide reservoir for acute kidney injury therapy. Elife. 2023;12:e84820. https://doi.org/10.7554/eLife.84820.
31. Huang A, Liu Y, Qi X, Chen S, Huang H, Zhang J, et al. Intravenously transplanted mesenchymal stromal cells: a new endocrine reservoir for cardioprotection. Stem Cell Res Ther. 2022;13(1):253. https://doi.org/10.1186/s13287-022-02922-z.
32. Liang L, Li Z, Ma T, Han Z, Du W, Geng J, et al. Transplantation of human Placenta-Derived mesenchymal stem cells alleviates critical limb ischemia in diabetic nude rats. Cell Transpl. 2017;26(1):45–61. https://doi.org/10.3727/096368916X692726.
33. Zheng J, Lu T, Zhou C, Cai J, Zhang X, Liang J, et al. Extracellular vesicles derived from human umbilical cord mesenchymal stem cells protect liver ischemia/reperfusion injury by reducing CD154 expression on CD4 + T cells via CCT2. Adv Sci (Weinh). 2020;7(18):1903746. https://doi.org/10.1002/advs.201903746.
34. Madhusudhan T, Wang H, Dong W, Ghosh S, Bock F, Thangapandi VR, et al. Defective podocyte insulin signalling through p85-XBP1 promotes ATF6-dependent maladaptive ER-stress response in diabetic nephropathy. Nat Commun. 2015;6:6496. https://doi.org/10.1038/ncomms7496.
35. Shahzad K, Bock F, Al-Dabet MM, Gadi I, Kohli S, Nazir S, et al. Caspase-1, but not Caspase-3, promotes diabetic nephropathy. J Am Soc Nephrol. 2016;27(8):2270–5. https://doi.org/10.1681/asn.2015060676.
36. Alicic RZ, Rooney MT, Tuttle KR. Diabetic kidney disease: challenges, progress, and possibilities. Clin J Am Soc Nephrol. 2017;12(12):2032–45. https://doi.org/10.2215/cjn.11491116.
37. Ji C, Zhang J, Shi H, Chen B, Xu W, Jin J, et al. Single-cell RNA transcriptomic reveal the mechanism of MSC derived small extracellular vesicles against DKD fibrosis. J Nanobiotechnol. 2024;22(1):339. https://doi.org/10.1186/s12951-024-02613-2.
38. Xia L, Yang M, Zang N, Song J, Chen J, Hu H, et al. PEGylated beta-Cell-Targeting exosomes from mesenchymal stem cells improve beta cell function and quantity by suppressing NRF2-Mediated ferroptosis. Int J Nanomed. 2024;19:9575–96. https://doi.org/10.2147/IJN.S459077.
39. Banerjee A, Singla DK. MSC exosomes attenuate sterile inflammation and necroptosis associated with TAK1-pJNK-NFKB mediated cardiomyopathy in diabetic ApoE KO mice. Front Immunol. 2024;15:1348043. https://doi.org/10.3389/fimmu.2024.1348043.
40. Liu L, Chen Y, Li X, Wang J, Yang L. Therapeutic potential: the role of mesenchymal stem cells from diverse sources and their derived exosomes in diabetic nephropathy. Biomed Pharmacother. 2024;175. https://doi.org/10.1016/j.biopha.2024.116672.
41. Mahtal N, Lenoir O, Tinel C, Anglicheau D, Tharaux PL. MicroRNAs in kidney injury and disease. Nat Rev Nephrol. 2022;18(10):643–62. https://doi.org/10.1038/s41581-022-00608-6.
42. Tsai YC, Kuo MC, Hung WW, Wu PH, Chang WA, Wu LY, et al. Proximal tubule-derived exosomes contribute to mesangial cell injury in diabetic nephropathy via miR-92a-1-5p transfer. Cell Commun Signal. 2023;21(1):10. https://doi.org/10.1186/s12964-022-00997-y.
43. Ning S, Chen Y, Li S, Liu M, Liu H, Ye M, et al. Exosomal miR-99b-5p secreted from mesenchymal stem cells can retard the progression of colorectal cancer by targeting FGFR3. Stem Cell Rev Rep. 2023;19(8):2901–17. https://doi.org/10.1007/s12015-023-10606-1.
44. Wei F, Liu Y, Guo Y, Xiang A, Wang G, Xue X, et al. miR-99b-targeted mTOR induction contributes to irradiation resistance in pancreatic cancer. Mol Cancer. 2013;12:81. https://doi.org/10.1186/1476-4598-12-81.
45. Juliana Doblas Massaro 1, Matheus Costa CDP, Silva 2 E. Cinthia Caroline Alves 2, Geraldo Aleixo Passos 3, Elza Tiemi Sakamoto-Hojo 4, Wallace Rodrigues de Holanda Miranda 5, Nathalia Joanne Bispo Cezar 2, Diane Meyre Rassi 2, Felipe Crispim 6, Sergio Atala Dib 6, Maria Cristina Foss-Freitas 5, Daniel Guariz Pinheiro 7, Eduardo Antônio Donadi Post-transcriptional markers associated with clinical complications in Type 1 and Type 2 diabetes mellitus. *Mol Cell Endocrinol, 15*(490), 1–14. https://doi.org/10.1016/j.mce.2019.03.008
46. Ruan H, Shi H, Luan W, Pan S. Bone marrow mesenchymal stem cell-derived Exosomal microRNA- 99b-5p promotes cell growth of high Glucose-treated human umbilical vein endothelial cells by modulating THAP domain containing 2 expression. Curr Stem Cell Res Ther. 2024. https://doi.org/10.2174/0115748888x272011231128073104.
47. Zhang Y, Zhao S, Wu D, Liu X, Shi M, Wang Y, et al. MicroRNA-22 promotes renal tubulointerstitial fibrosis by targeting PTEN and suppressing autophagy in diabetic nephropathy. J Diabetes Res. 2018;2018:1–11. https://doi.org/10.1155/2018/4728645.
48. Wang X, Gao Y, Tian N, Zhu Z, Wang T, Xu J, et al. Astragaloside IV represses high glucose-induced mesangial cells activation by enhancing autophagy via SIRT1 deacetylation of NF-κB p65 subunit. Drug Des Devel Ther. 2018;12:2971–80. https://doi.org/10.2147/dddt.S174058.
49. Yasuda-Yamahara M, Kume S, Maegawa H. Roles of mTOR in diabetic kidney disease. Antioxidants. 2021;10(2). https://doi.org/10.3390/antiox10020321.
50. Lloberas N, Cruzado JM, Franquesa M, Herrero-Fresneda I, Torras J, Alperovich G, et al. Mammalian target of Rapamycin pathway Blockade slows progression of diabetic kidney disease in rats. J Am Soc Nephrol. 2006;17(5):1395–404. https://doi.org/10.1681/asn.2005050549.
51. Mori H, Inoki K, Masutani K, Wakabayashi Y, Komai K, Nakagawa R, et al. The mTOR pathway is highly activated in diabetic nephropathy and Rapamycin has a strong therapeutic potential. Biochem Biophys Res Commun. 2009;384(4):471–5. https://doi.org/10.1016/j.bbrc.2009.04.136.
52. Su W, Yin Y, Zhao J, Hu R, Zhang H, Hu J, et al. Exosomes derived from umbilical cord-derived mesenchymal stem cells exposed to diabetic microenvironment enhance M2 macrophage polarization and protect against diabetic nephropathy. Faseb J. 2024;38(14):e23798. https://doi.org/10.1096/fj.202400359R.

Publisher's note